Journal of Sea Research 199 (2024) 102498

Contents lists available at ScienceDirect

Journal of Sea Research

journal homepage: www.elsevier.com/locate/seares

Fluxes of nitrogen and phosphorus in fouling communities on artificial offshore structures

Joop W.P. Coolen [a,*], Babeth van der Weide [a], Oliver Bittner [a], Ninon Mavraki [a], Mandy Rus [a], Johan van der Molen [b], Rob Witbaard [b]

[a] Wageningen Marine Research, Ankerpark 27, 1781 AG Den Helder, the Netherlands
[b] Royal Netherlands Institute for Sea Research, P.O. Box 59, 1790AB Den Burg, the Netherlands

ARTICLE INFO

Keywords:
Shipwrecks
Offshore wind farms
Benthos
Nitrogen
Phosphate
Biogeochemical cycle

ABSTRACT

The number of offshore artificial structures in the North Sea is continuously increasing. Apart from the structures that have been added to the marine environment accidentally (e.g., shipwrecks), structures are also deliberately developed to meet the increasing needs for renewable energy. These structures provide habitat for fouling organisms. The fouling communities vary in abundance and composition based on location, depth, and structure age. Most fouling species filter particles from the water column, changing phytoplankton production and affecting larval settlement success, while releasing ammonium that can fuel phytoplankton growth as well as (pseudo)faeces that enriches the seabed, changing local biogeochemical cycles.

Our study used in-situ incubation chambers to investigate oxygen, nitrogen, and phosphate fluxes associated with fouling organisms to improve understanding of these changes in biogeochemical cycles. Divers used incubation chambers (domes) on shipwrecks in the southern North Sea where over 55 years mature fouling communities have established. A series of water samples was collected from each dome during deployment to measure the change in concentration of ammonium, nitrite, nitrate, and phosphate. All fauna enclosed in the domes was collected after each measurement for further analysis.

The full macrofauna dataset contained 65 unique species on 4 shipwrecks (25 to 50 species per sample). Abundance ranged from 2187 to 59,427 individuals per sample (683 cm^2). On average, a decrease in oxygen concentration of 126 μmol/g ash free dry weight/h was found. The sequential water samples also showed clear changes in nutrient concentration with time in all incubations. The largest changes were observed with high fouling community abundances and biomass. Ammonium, nitrite, and phosphate always increased, with 1.5-to-5-fold increases from start to end of the incubation, while for nitrate both an efflux and influx were measured. Oxygen decreased in all incubations. Mean fluxes (all in μmol per m^2 per hour with standard error) were significant for ammonium (945 ± 300), nitrite (80 ± 30), phosphate (61 ± 8), and oxygen (−11,794 ± 3289), but not for nitrate (−206 ± 122). Per gram AFDW, only ammonium (12.7 ± 3.5) and oxygen (−126 ± 48) had fluxes that differed significantly from zero.

Compared to average seabed (sandy bottom) oxygen demand and community fluxes from previous studies, the observed fluxes were high. Our findings resembled those from temperate biogenic reef studies. Further data collection across a larger spatial and temporal scale is needed to fully understand offshore structure effects on marine environments.

1. Introduction

As a result of worldwide renewable energy targets, the number of artificial offshore structures has been rapidly increasing in recent years (Fowler et al., 2018; World Forum Offshore Wind, 2023; Xu et al., 2022). In 2019, almost 7000 offshore wind turbines were present worldwide (Zhang et al., 2021) and in 2022 alone, a record number of over 1500 wind turbines were added to global marine waters. In the North Sea, a total of 25,000 offshore wind turbines is expected to be installed before 2050 (de Vrees, 2019). Other renewable energy devices, such as floating solar panels (Hooper et al., 2021; Vlaswinkel et al., 2023), wave energy converters (Nall et al., 2017; Witt et al., 2012) and many other initiatives

* Corresponding author.
E-mail address: joop.coolen@wur.nl (J.W.P. Coolen).

https://doi.org/10.1016/j.seares.2024.102498
Received 14 December 2023; Received in revised form 12 March 2024; Accepted 9 April 2024
Available online 10 April 2024

(Vanaverbeke et al., 2019) will also add to the number of artificial structures in the marine environment. Furthermore, anthropogenic structures with other functions are also present, such as 12,000 offshore oil and gas structures worldwide (McLean et al., 2022), many thousands of navigational aids (Coolen et al., 2020b), aquaculture farms (Jansen et al., 2016) and shipwrecks (Lengkeek et al., 2013). Finally, dedicated artificial reefs are also introduced to enhance biodiversity or as a measure to replace functions provided by natural reefs that have been diminished. Artificial structures usually differ from each other in material (e.g. steel, concrete, etc.), orientation and location within the marine environment, depending on their purpose or whether they have been placed in the environment deliberately or accidentally. For example, offshore wind turbine foundations and oil and gas platforms traverse the full water column, navigational buoys are floating on the water surface, while shipwrecks are situated on the seabed, and are mainly horizontally stretched.

The addition of artificial structures introduces hard substrate, increasing habitat heterogeneity and promoting colonisation by marine fouling communities and associated species (Degraer et al., 2020; Schutter et al., 2019). In the North Sea, this epibenthic fouling fauna is dominated by blue mussels, amphipods and anemones (Coolen et al., 2020c; Krone et al., 2013; Zupan et al., 2023), which vary in abundance depending on location, depth and age of the structure (Coolen et al., 2022; Degraer et al., 2020). The associated community is highly biodiverse and contains species which are absent in the surrounding sediment (Coolen et al., 2020a). As a result, by including such artificial hard substrate structures the local macrofauna community is strongly enriched, an effect which increases during the life span of a structure (Li et al., 2023). The abundance of the fouling species can reach densities of over 10^6 individuals per m^2 (Coolen et al., 2020c; Luttikhuizen et al., 2019) with a wet weight biomass of over 50 kg per m^2 in some cases (Krone et al., 2013), much higher than observed in the surrounding seabeds (Coolen et al., 2020a). Similar communities to those found on shipwrecks are observed on the deeper parts of wind turbine foundations. Both reef types show dominance of *Metridium senile* and *Jassa herdmani*. The primary difference between shipwrecks and wind turbines is the penetration of the full water column by turbine foundations, which is absent on all offshore shipwrecks in the southern North Sea. The shallow parts of turbine foundations are dominated by blue mussels (*Mytilus edulis)*, which are rare on shipwrecks (Coolen et al., 2020b, 2022; Hiscock, 1981; Krone and Schröder, 2011; Leewis and Waardenburg, 1991; Lengkeek et al., 2013; Massin et al., 2002; Zintzen et al., 2006; Zupan et al., 2023).

After the introduction of artificial structures in a mainly sandy seabed environment, the local food web changes due to a shift in species composition and the way organic matter is processed (Voet et al., 2023a, 2023b). The fouling communities feed directly from the readily available stock of phyto-, zoo- and ichthyoplankton provided by a continuous flow of water along the structures (Coolen et al., 2020a; Mavraki et al., 2020b, 2022). This may lead to a decrease in phytoplankton primary production (Slavik et al., 2019) and planktonic larval settlement success (Dannheim et al., 2020). By filter feeding, the epibenthic community also removes organic and inorganic matter from the water (Mavraki et al., 2020a). Simultaneously, the species and their biofilms excrete inorganic nitrogen, mainly in the form of ammonium which, either directly or after conversion to nitrite and nitrate, becomes available to the phytoplankton community (Smith et al., 2014; Voet et al., 2023b). Since nitrate as well as phosphate can be limiting nutrients for phytoplankton communities in the North Sea (Burson et al., 2016; Peeters and Peperzak, 1990), this would also influence phytoplankton growth. Fouling communities may therefore alter the ecosystem metabolism and biogeochemical cycling (De Borger et al., 2021b; Wilking et al., 2023). The biogeochemical cycle of fouling communities and surrounding waters has been studied using models (De Borger et al., 2021b), or lab experiments (Babcock et al., 2020; Voet et al., 2023a; Wilking et al., 2023). Fluxes have been measured previously in temperate biogenic reefs (Kellogg et al., 2013) or using sandy seabed communities from Portugal (Falcão et al., 2007) or the North Sea (Bratek et al., 2020; De Borger et al., 2021a). Finally, benthic fluxes have also been estimated in situ at a subtropical natural stony reef in the USA (Hopkinson et al., 1991). However, to date, no in situ studies have been performed on the fluxes of nutrients from fouling communities on offshore artificial structures in the North Sea.

The aim of this study was to provide novel data on benthic fluxes of offshore fouling communities in the North Sea. We used a newly designed incubation chamber (dome) to measure in situ oxygen, nitrogen, and phosphate fluxes associated with fouling communities present on artificial structures in the North Sea. The incubations were performed without removing the organisms from their natural environment, thus providing fluxes based on near-natural conditions, and assuring that the organisms experienced limited disturbances. We show that fluxes of ammonium, nitrite, nitrate, and phosphate are high compared to fluxes associated with sandy seabed communities.

2. Methods

2.1. Locations

Incubations were carried out in June 2021 on four offshore shipwrecks in the southern North Sea (Fig. 1). In the Netherlands, access to offshore wind farm (OWF) turbine foundations is strictly prohibited and non-essential diving activities are severely limited by regulations, making scientific diving in Dutch wind farms impossible in practice. Communities on shipwrecks are similar to those on OWF foundations in the same region, with identical dominant species at depths away from the water surface (Coolen et al., 2012, 2020a, 2020c; Gmelig Meyling et al., 2012; Lengkeek et al., 2013; van der Stap et al., 2016). Therefore, shipwreck fouling communities were measured, which serve as a proxy for the fouling communities on OWF turbine foundations.

The area of the wrecks is characterised by a sandy seabed with water depths ranging between 30 and 37 m (Table 1). All four shipwrecks were made of steel and sank between 1915 and 1966, all >55 years ago, which is significantly older than any current offshore wind farm. All were observed to have a mature fouling community. The wrecks are in an area of the North Sea that is considered well mixed, with insignificant differences in temperature between surface and bottom water (Holt and James, 1999). The salinity in the area of the wrecks during sampling was 35 parts per thousand (conductivity of 53 mS/cm), with a water temperature of 14 °C. Typical chlorophyll *a* values for the region are <1 μg.l^{-1} in winter and 2–5 μg.l^{-1} in summer, with a spring bloom at 5–40 μg.l^{-1} in April (Rijkswaterstaat, 2024). Some light is known to penetrate the water down to the wrecks, allowing diver's vision without artificial light, but since macroalgae were not observed on wrecks in this region light availability was considered to be too low for macroalgae to survive (personal observations Joop Coolen).

2.2. Incubations

2.2.1. Dome system

Incubations were carried out using an in-situ hemispherical respiration chamber (hereafter called dome), designed to measure changes in nutrient and oxygen concentrations within the time frame of a 45-min wreck dive. The dome shape minimises the outer dimensions of the chamber to allow easier handling by divers and avoids dead space in corners, thus optimising internal mixing, while maximising its content volume for stable measurements. Dome size was based on the average adult individual oxygen consumption of *Jassa herdmani* in densities as typically observed on offshore wind turbine foundations, which was much higher than that of the other dominant species (*Metridium senile* and *Mytilus edulis*; unpublished data by Ninon Mavraki; (Dannheim et al, submitted). These data on individual O_2 consumption rates were extrapolated to O_2 use per m^2, based on average densities in data

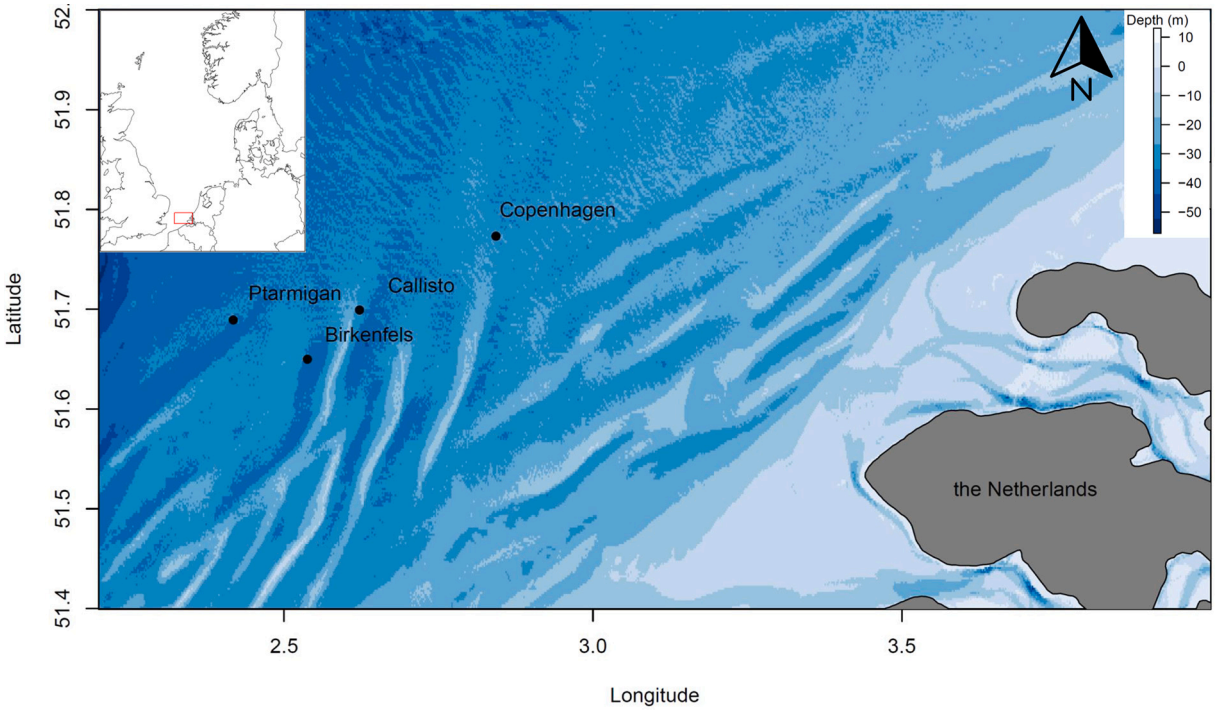

Fig. 1. Measurement locations (black points with shipwreck's name) in the southern North Sea with bathymetry. Inset map: greater North Sea with study area (small red box). (For interpretation of the references to colour in this figure legend, the reader is referred to the web version of this article.)

Table 1
Location data with sample incubation number (ID), location name, geographic position (WGS84, decimal degrees), year of sinking (Year), sampling date, local water depth [Depth seabed; referring to the Lowest Astronomical Tide Datum (EMODnet, 2019)] and depth below surface at which the incubation was performed (Depth, as measured by the diver), total incubation time in minutes (Time) and number of minutes between water samples (Int).

ID	Name	Latitude	Longitude	Year	Sample date	Depth seabed	Depth	Time	Int
1	Ptarmigan	51.689	2.418	1915	21 June 2021	35	35	18	6
2	Callisto	51.699	2.622	1959	24 June 2021	30	24	24	8
3	Callisto	51.699	2.622	1959	24 June 2021	30	29	27	9
4	Callisto	51.699	2.622	1959	25 June 2021	30	27	30	10
5	Birkenfels	51.650	2.538	1966	25 June 2021	37	31	30	10
6	Copenhagen	51.773	2.843	1917	26 June 2021	31	27	27	9

available from fouling communities on gas platforms and OWF turbine foundations (Coolen et al., 2020c, 2022). This rate (11.7 mmol m^{-2} h^{-1} on average) was used to calculate the dome size needed to attain an O_2 reduction of <30% during a single incubation, to prevent a change in behaviour of the community due to oxygen depletion, resulting in a hemisphere with a diameter of 30 cm.

The domes were built using a 3 mm thick transparent acrylate hemisphere of 295 mm inner bottom diameter, with a 15 mm wide rim, extending outwards from the dome bottom. The surface included inside the dome was 683 cm^2. On the rim a soft rubber seal was clamped, to which a soft rubber hose was glued along the length of the seal, creating a highly flexible circular seal of 20 mm (compressed) to 50 mm (uncompressed) height. This high flexibility was essential to allow the seal to close on the rough surfaces of shipwrecks, which can be severely corroded after decades in sea water. Total volume contained in the dome without seal was 6.8 l. Volume contained in the dome with seal (as placed on the shipwrecks) was between 8.2 and 10.3 l, depending on seal compression. Seal height was observed to vary between placements and along the seal within placements, due to the surface roughness of the corroded steel. Since the height was not quantified in situ, it was assumed the seal was compressed slightly over 50% of its maximum and the typical volume contained in the dome was assumed to be 9 l.

The dome was mounted with a 4 V, 100 l h^{-1} capacity pump (model DC30A-0406, BLDC pump Co. Ltd., China) integrated in a custom-made housing with an on/off switch and three rechargeable 3.7 V batteries wired in parallel. The pump could operate approximately 18 h on a single charge. The pump housing was mounted at an angle of 35 degrees away from the top of the dome, with the pump outflow in a horizonal direction along the dome wall, creating a circular horizonal flow inside the dome. Flow speed when placed on a surface was calculated by observing a neutrally buoyant substance rotating with the flow inside the dome, and measuring the time it took to perform a full rotation. This was estimated to be ~1 knot (~0.51 m s^{-1}), which is within the range of current speeds observed in the southern North Sea. Mixing was tested visually in the laboratory prior to offshore measurements, by injecting a dye into the dome while the pump was activated and observing the dilution over time. The dye diluted within minutes to a visually homogenous concentration throughout the dome. Thus, the dome was assumed to be well mixed during incubations.

An optical dissolved oxygen (DO) sensor with wiper (RINKO W model AROW2-USB by JFE Advantech Co., Ltd., Japan) was mounted on top of the dome. The sensor was set to a sampling rate of 1 measurement per second, starting before divers entered the water and stopping after resurfacing. The actual incubation period was selected from the stored data in post processing. O_2 concentrations were provided as mg per l, which was calculated from the saturation percentage (Weiss, 1970) using the manufacturers INFINITY SERIES acquisition tools software (version 1.12). The sensor was calibrated prior to the cruise following

the manufacturers protocol, by two-point calibration in oxygen saturated water (attained by bubbling air trough it for >20 min) as well as anoxic water (attained by adding an excess of sodium sulphite and subsequent magnetic stirring).

The dome was further fitted with a Luer lock port with cap, to allow the collection of water samples during incubation. To stabilise the dome and push the dome towards the steel surface to attain a proper seal, bungee cords were fitted across the dome, which were attached to neodymium magnets, rated at a strength of 100 kg each. The magnets were fitted with handlebars to facilitate placement on and removal from the wreck by the diver (Fig. 2).

2.2.2. Dome placement & fauna sampling by divers

The field work was carried out by divers. We collaborated with a group of wreck divers of the Dutch 'Dive the North Sea Clean foundation', who visit shipwrecks to remove lost fishing gear and monitor presence of reef dwelling species as part of a citizen science project (Coolen et al., 2016; Kerckhof et al., 2018). Local tidal current conditions reach 1.9 knots, severely restricting diving time in the southern North Sea, as scuba divers can safely endure currents of <0.6 knots. This safety requirement limited dive time to a maximum of 45 min on the wreck around slack tide. The team visited new shipwrecks daily and relocated between most dives. Therefore, each measurement had to be carried out within a single dive, even though the dive team did visit locations repeatedly.

After arriving on the shipwreck, the diver selected an area of steel large enough to fit the dome, flat enough to attain a proper seal, and covered with a fouling community which appeared to be representative of the average community on the surrounding wreck sections. Then a ring-shaped area where the dome seal would touch the steel was cleaned of all fauna, and where possible protruding corrosion spots were removed. Care was taken to limit disturbance of the fauna inside the ring. Then the diver placed the dome over the fauna in the ring, pulling the magnets outwards from the dome during placement, pushing the magnet on the steel of the wreck, and tightening the bungee cords, thus creating a downward force on the dome pressing the seal on the steel surface. A dive light was used to shine on the seal-to-steel connection around the dome edge, while the diver looked for traces of light inside the dome. If light penetration was observed, the seal was adjusted to ensure improved contact with the steel around the dome, such that the water inside the dome was isolated from the environment. This installation process took approximately 5 min. Then the dome was covered with a red cloth to prevent O_2 production by algae or phytoplankton, even though significant presence of algae was not expected, based on the experience of the authors (personal observations Joop Coolen; Fig. 3).

The moment when the dome was covered was considered the start of the incubation. A timer was activated on a dive computer to mark this as $T = 0$. Total incubation time depended on the maximum diving time and was between 18 and 30 min, approximately 15 min less than the total diving time. At the end of the incubation, the dome was removed and stowed, the fauna underneath was scraped off using a putty knife and collected in a macrofauna net (mesh size 0.5 mm). This was also stowed, and the dive ended. Back on board the fauna sample was deposited in a labelled container and conserved using 99% ethanol. The ethanol was replaced after 24 h to ensure the percentage was >70%, which was considered sufficient for long term storage.

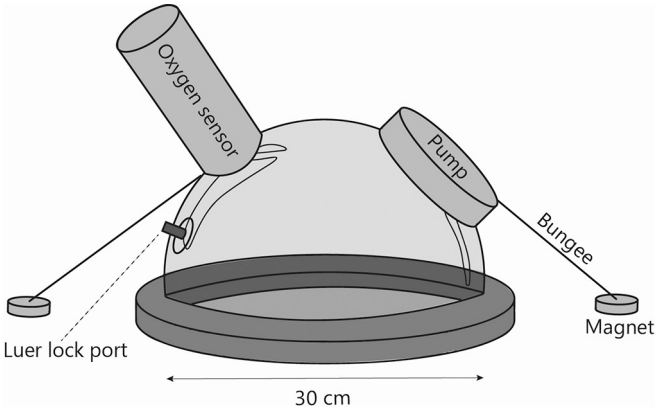

Fig. 2. Simplified sketch of the dome layout (not to scale).

2.2.3. Water samples

During incubation, water samples were collected using four 60 ml syringes attached to a Luer-Lock port in the dome. For each water sample (timepoint) a separate syringe was used. Syringes were locked with luer lock caps. Depending on the depth, the diver would take water samples at intervals of ([maximum diving time – 15 min] / 3), attaining a total of 4 water samples per incubation (Table 1). This sampling of 240 ml water in total per incubation was assumed to have a negligible effect on the concentration and was not further accounted for during data analysis.

Within 30 min after the dive ended, the water samples were processed on board. A sterile Acrodisc® PF 32 mm Syringe Filter with 0.8/0.2 µm Supor® Membrane (PALL Life Sciences) was attached to the syringe containing the water sample. A minimum of 2 ml of water was pushed through the filter before a sample was deposited in a 6 ml plastic pony vial. The vials were rinsed three times with ~1 ml of the Acrodisc filtered sample water and then filled to the 6 ml line, leaving headspace under the rinsed lid. All vials were stored at −20 °C.

2.3. Lab analysis

2.3.1. Macrofauna

Analysis in the laboratory was carried out following methods applied to similar samples in earlier studies (Coolen et al., 2015, 2020a, 2020b, 2022). All fauna samples were first pre-sorted into practical taxonomic groups, after which they were identified to the lowest taxonomic level possible, preferably species, using the World Register of Marine Species (WoRMS Editorial Board, 2022) as a reference for taxonomic nomenclature. Samples containing >200 individuals of one species were sorted, removing all species except the abundant (>200 ind.) species, which was left in the main sample. Then the remaining sample was subsampled using a Motoda-box sample splitter (Motoda, 1959) to a level at which between 100 and 200 individuals of the species were left in the sub-sample. Next, the sub-sample was processed like the full sample, noting the sub-sample fraction in the dataset for all specimens identified in the sub-sample. All taxa were wet weighed, then dried at 60 °C for 72 h and weighed after acclimatisation to room temperature in a desiccator. Then incinerated at 560 °C for a minimum of 4 h, and then weighed again after acclimatisation to room temperature in a desiccator to obtain the ash weight.

2.3.2. Water analysis

The water samples were analysed in the nutrient laboratory of the Royal Netherlands Institute of Sea Research following the protocol by Hydes et al. (2010), using a Continuous Segmented Flow analyser 'TrAAcs 800'. Calibration was done using additions of concentrated stock standard solutions in Low Nutrient Seawater. Orthophosphate (henceforth named phosphate) was measured by formation of a blue reduced Molybdophosphate-complex at pH 0.9–1.1. Potassium Antimonyltartrate was used as the catalyst and ascorbic acid as a reducing agent. The absorbance was measured at 880 nm (Murphy and Riley, 1962). Ammonium reacts with phenol and sodium-hypochlorite buffered with citrate at pH 10.5 to form an indo-phenol-blue complex. Citrate was used as a buffer. The blue colour was measured at 630 nm (Helder and De Vries, 1979). Nitrite was measured by diazotation of nitrite with sulfanylamide and N-(1-naphtyl)-ethylene diammonium dichloride to form a pink dye measured at 550 nm. Nitrate plus nitrite

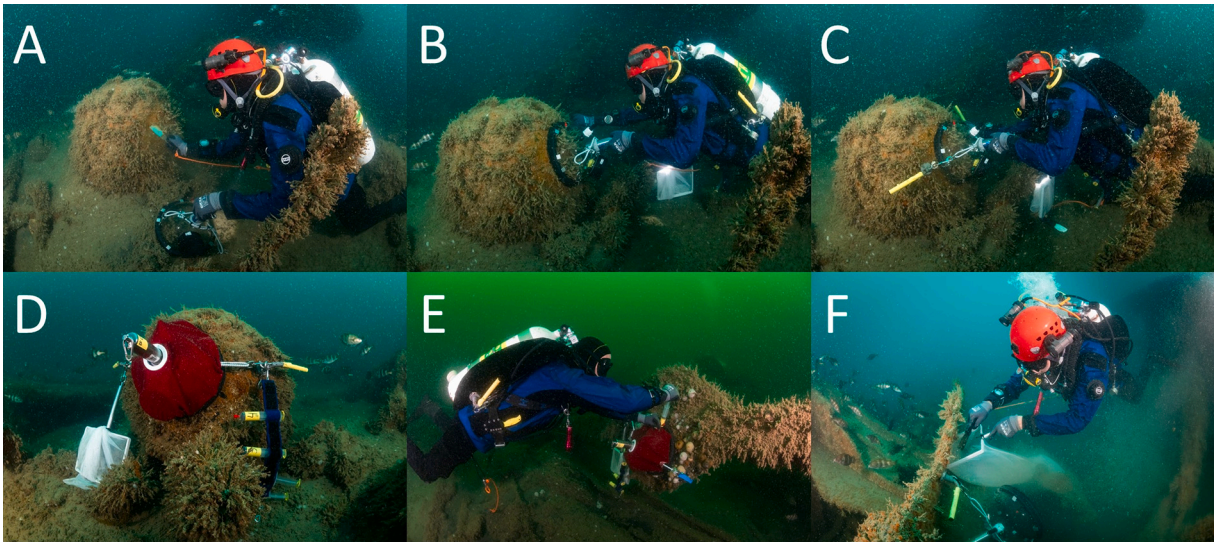

Fig. 3. Incubation process. A: diver selects an area and removes ring of fauna. B: The dome is placed. C: Magnets (yellow bars) are placed to hold dome in place. D: The dome is covered with a red cloth. E: Water sample is taken using a syringe. F: after incubation the fauna is collected in a net. Photos by Joost van Uffelen. (For interpretation of the references to colour in this figure legend, the reader is referred to the web version of this article.)

(NO3 + NO2) was first buffered with an imidazol buffer at pH 7.5 and reduced by a copperised cadmium column to Nitrite. Nitrite was then diazotized with sulphonyl-amide and naphthyl-ethylene-diamine to form a pink coloured complex and measured at 550 nm. Nitrate was subsequently calculated by subtracting the nitrite value of the nitrite channel from the 'NO3 + NO2' value (Grasshoff et al., 1983).

2.4. Data analysis

All data analysis was performed in R (R Core Team, 2022) and RStudio (RStudio, 2022). The analysis was performed in multiple steps. All sub sampled fauna data (counts and weights) were multiplied by the sub sampling factor of the sample to obtain the full sample equivalent. For each sample, total biomass (ash free dry weight [AFDW] based on the dry weight – ash weight in grams) and total number of individuals were calculated, as well as the mean individual AFDW per sample (AFDW/total individuals). All nutrient sample data were converted to µM (µmol per litre) and to total µmol present in the dome water (9 l). A data exploration was performed, following Zuur et al. (2010). The presence of outliers, multi-collinearity, and relations between number of individuals and biomass per sample, time of incubation and water sample variables was assessed using Cleveland dotplots (Cleveland, 1985), pair plots, and multi-panel scatterplots, using the ggplot2 package (Wickham, 2009). For each water sample variable (total µmol in the dome) in relation to time a linear model, using the lm function in R, was created for each incubation. The slope and standard error of each model were combined with the community data for the corresponding sample to allow modelling of relations between fluxes and community data, such as biomass or abundance. A data exploration was performed on the newly generated data, following methods described above. The slopes of the models per nutrient were modelled against the weight of the samples using a linear model (lm function), to obtain a typical change in µmol per gram of biomass per unit of time (flux). The slopes and standard errors of the models per water variable were also averaged to obtain a typical flux per dome area per unit of time, which was then converted into a flux in µmol per m^2 per unit of time. Whether these averages differed significantly from zero was assessed using a *t*-test (t-test function). The resulting data were plotted using ggplot2.

3. Results

3.1. Macrofauna communities

In total, 65 unique species were observed in six samples. The number of species per sample varied between 25 and 50. The number of individuals in a sample varied between 2187 and 59,427 on a sampled area or 683 cm^2, which is 31,997–869,460 individuals per m^2, respectively. Wet weight and ash free dry weight per sample ranged from 7.27 g to 107.7 g (wet) or 0.76 g to 10.4 g (AFDW). In all samples combined, Arthropoda were, by far, the most abundant phylum, followed by Annelida or Mollusca. Amphipoda made up an average of 86 ± 6% (standard error) of the total number of individuals in a sample, with a maximum of 96% in samples 1 and 6. Within Arthropoda, the amphipod *Jassa herdmani* (including juveniles), made up 57 to 99% of the individuals (Table 2). Considering ash free dry weight (AFDW), Arthropoda represented the highest weight in only 3 samples, while the other samples were dominated by Mollusca (1 sample) and Cnidaria (2 samples; Fig. 4). The complete macrofauna dataset is available as online supplement S1.

The Callisto wreck was sampled 3 times (sample ID 2–3-4). The number of individuals per sample varied between 2187 (ID4) and 45,152 (ID3) while AFDW varied between 0.7 g (ID2) and 4.8 g (ID3). This difference was caused mainly by the much higher number of Amphipoda in ID3, which was 14 times that of ID2 and 34 times that of ID4, with similar ratios in AFDW.

3.2. Fluxes of oxygen and nutrients

In oxygen and all nutrients during most incubations, there was a change in concentration with time (Fig. 5). In general, the largest change (steepest model slope) was associated with the highest observed abundances and biomasses of the fouling community. Oxygen decreased in all incubations ($-11{,}794 \pm 3289$ µmol $m^{-2}.hr^{-1}$ on average) and showed a relation with ash free dry weight biomass of the community (-126 ± 48 µmol/$g.hr^{-1}$, $p = 0.06$, $R^2 = 0.54$).

For ammonium, nitrite, and phosphate there was a statistically significant ($p < 0.05$) increase with time in most incubations. For nitrate, there was a small statistically significant increase with time in 2 incubations and no statistically significant change in 4 incubations. The mean flux of these nutrients in all incubations was significantly different

Table 2
Macrofauna data averaged for all samples (sampled area 683 cm^2 per sample), with taxon names grouped on Phylum level, abundance (mean number of individuals or size (cm^2) of colonies ± standard error for all samples) and mean ash free dry weight (g) ± standard error for all samples ("–"indicates no AFDW was measured).

Phylum / Taxon	Abundance	AFDW (g)
Annelida		
Autolytinae	1 ± 1	–
Capitella sp.	3.5 ± 2.58	–
Caulleriella sp.	0.5 ± 0.5	–
Cirratulidae	30.17 ± 18.49	0.002 ± 0.002
Cirratulus cirratus	1 ± 0.82	0.0003 ± 0.0003
Cirratulus sp.	1.83 ± 1.83	–
Dipolydora caulleryi	0.33 ± 0.33	–
Dipolydora coeca	2 ± 1.13	–
Enchytraeidae	36 ± 36	–
Eteone flava	0.33 ± 0.21	–
Eulalia sp.	0.33 ± 0.33	–
Eulalia viridis	0.33 ± 0.21	–
Eumida sanguinea	0.83 ± 0.54	0.0003 ± 0.0003
Gattyana cirrhosa	0.17 ± 0.17	–
Glyceridae	0.17 ± 0.17	–
Harmothoe extenuata	2.17 ± 1.8	0.0054 ± 0.0047
Hesionidae	21.5 ± 21.5	–
Lanice conchilega	3 ± 2.45	0.0014 ± 0.0009
Lepidonotus squamatus	0.83 ± 0.65	0.0041 ± 0.0031
Lumbrineris cingulata	0.33 ± 0.33	–
Marphysa sanguinea	0.17 ± 0.17	0.0023 ± 0.0023
Marphysa sp.	0.33 ± 0.33	–
Mediomastus fragilis	12.17 ± 11.97	–
Myrianida sp.	0.33 ± 0.33	–
Nephtys sp.	1.67 ± 1.67	0.0004 ± 0.0004
Nereididae	0.33 ± 0.21	–
Nereis zonata	0.33 ± 0.21	–
Notomastus latericeus	0.17 ± 0.17	–
Ophryotrocha sp.	0.33 ± 0.33	–
Parasabella sp.	0.67 ± 0.67	–
Pectinariidae	7.5 ± 4.76	0.0009 ± 0.0009
Perkinsiana rubra	0.17 ± 0.17	–
Pholoe inornata	0.5 ± 0.5	–
Phyllodoce maculata	2.67 ± 2.47	–
Phyllodoce sp.	47 ± 28.16	–
Phyllodocidae	2.17 ± 1.97	–
Pilargidae	0.17 ± 0.17	–
Polycirrus sp.	0.67 ± 0.67	–
Polynoidae	89.17 ± 56.89	0.0321 ± 0.0202
Procerastea halleziana	52.83 ± 44.75	–
Protocirrineris sp.	20 ± 20	0.0034 ± 0.0035
Psamathe fusca	0.17 ± 0.17	–
Sabellaria spinulosa	93.67 ± 47.4	0.0031 ± 0.0031
Sabellida	0.33 ± 0.33	–
Sipuncula	0.17 ± 0.17	–
Spiophanes bombyx	0.17 ± 0.17	–
Spirobranchus lamarcki	4.5 ± 1.59	0.0024 ± 0.0012
Spirobranchus sp.	0 ± 0	–
Spirobranchus triqueter	77 ± 41.15	0.0593 ± 0.0343
Syllis armillaris	1 ± 1	0.0003 ± 0.0003
Syllis gracilis	8.5 ± 6.52	0.0011 ± 0.0011
Terebellida	19 ± 19	0.0056 ± 0.0056
Terebellidae	10.33 ± 5.64	0.0007 ± 0.0007
Arthropoda		
Apseudopsis latreillii	2 ± 2	0.0008 ± 0.0008
Balanomorpha	16.5 ± 7.07	–
Balanus crenatus	165.67 ± 106.12	–
Caprella sp.	0.33 ± 0.33	–
Caprella tuberculata	2.67 ± 1.15	0.001 ± 0.0005
Caprellidae	0.33 ± 0.21	–
Corophiidae	226.33 ± 97.42	–
Decapoda	0.17 ± 0.17	–
Ischyroceridae	12,099 ± 4856	0.0123 ± 0.0123
Jassa herdmani	11,241 ± 4458	1.9064 ± 0.8874
Jassa sp.	2.67 ± 2.67	–
Liocarcinus sp.	0.83 ± 0.54	0.0019 ± 0.0012
Lysianassa ceratina	5.5 ± 4.06	0.0204 ± 0.0162
Macropodia rostrata	0.17 ± 0.17	0.0043 ± 0.0043
Monocorophium acherusicum	324 ± 207.18	–
Monocorophium sextonae	24 ± 20.96	–
Phtisica marina	13.83 ± 5.8	0.0045 ± 0.0022
Pilumnus hirtellus	8.67 ± 2.11	0.0124 ± 0.0035
Pisidia longicornis	101.67 ± 39.99	0.281 ± 0.1346
Sessilia	63.33 ± 63.33	–
Stenothoe monoculoides	33 ± 25.14	0.0002 ± 0.0002
Stenothoe valida	40.67 ± 26.65	0.0196 ± 0.0138
Stenothoidae	97 ± 67.8	–
Verruca stroemia	4 ± 4	–
Bryozoa		
Bugulina fulva	0.17 ± 0.17	–
Conopeum reticulum	0.17 ± 0.17	–
Crisia aculeata	0.5 ± 0.5	–
Disporella hispida	0.17 ± 0.17	–
Electra pilosa	9 ± 4.83	–
Oncousoecia dilatans	0.17 ± 0.17	–
Plagioecia sp.	0.17 ± 0.17	–
Scrupocellaria scruposa	2.83 ± 1.49	–
Smittina sp.	0.33 ± 0.21	–
Vesicularia spinosa	0.33 ± 0.21	–
Chordata		
Diplosoma listerianum	1 ± 1	–
Pomatoschistus sp.	0.33 ± 0.33	–
Cnidaria		
Abietinaria abietina	0.33 ± 0.21	–
Actiniaria	128.83 ± 29.62	0.5904 ± 0.3045
Bougainvilliidae	1.17 ± 0.6	–
Campanulariidae	0.83 ± 0.17	–
Nemertesia antennina	0.17 ± 0.17	–
Plumularia setacea	0.17 ± 0.17	–
Plumulariidae	0.33 ± 0.21	–
Sertularia sp.	0.33 ± 0.21	–
Sertulariidae	0.17 ± 0.17	–
Tubularia indivisa	216.67 ± 108.12	–
Echinodermata		
Amphipholis squamata	3.5 ± 2.73	0.0016 ± 0.0011
Asteroidea	22.83 ± 10.85	0.0052 ± 0.002
Diadematoida	0.67 ± 0.67	0 ± 0
Echinoidea	0.17 ± 0.17	–
Ophiothrix fragilis	59 ± 25.54	0.0365 ± 0.0209
Ophiuroidea	7 ± 2.67	–
Psammechinus miliaris	2 ± 0.73	0.0128 ± 0.0069
Mollusca		
Anomiidae	23.17 ± 21.01	0.0009 ± 0.0009
Buccinoidea	2.33 ± 2.14	0.0239 ± 0.0236
Cerithiopsis tubercularis	0.33 ± 0.33	0.0002 ± 0.0002
Crepidula fornicata	1.17 ± 0.65	0.0076 ± 0.0056
Epitonium clathratulum	2.83 ± 2.44	–
Euspira nitida	0.5 ± 0.34	0.0002 ± 0.0002
Gastropoda	0.67 ± 0.42	0.0016 ± 0.0011
Musculus subpictus	3 ± 1.51	0.0011 ± 0.0008
Mytilidae	305.33 ± 178.41	–
Mytilus edulis	64.83 ± 50.7	0.4513 ± 0.4115
Nudibranchia	1.83 ± 0.79	0.0032 ± 0.0032
Philine sp.	0.33 ± 0.33	–
Pusillina inconspicua	0.5 ± 0.34	–
Rissoidae	4 ± 3.11	–
Trivia sp.	0.83 ± 0.83	0.0093 ± 0.0093
Veneridae	1.33 ± 0.8	0.0007 ± 0.0005
Venerupis corrugata	0.33 ± 0.33	0.0052 ± 0.0052
Nemertea	5 ± 1.84	0.0086 ± 0.0047
Porifera		
Halichondria sp.	1.67 ± 1.67	–
Porifera	1 ± 0.82	–
Sycon ciliatum	1.33 ± 1.15	–

from zero ($p < 0.05$) in the case of ammonium (945 ± 300 [s.e.] μmol $m^{-2}.hr^{-1}$), nitrite (80 ± 30 μmol $m^{-2}.hr^{-1}$) and phosphate (61 ± 8 μmol $m^{-2}.hr^{-1}$) while no significant difference from zero was observed for nitrate (−206 ± 122 μmol $m^{-2}.hr^{-1}$). The mean ratio between N (ammonium + nitrite + nitrate) and P (phosphate) fluxes was 12 ± 5.1 (s.e.). Fluxes per gram AFDW were significantly different ($p < 0.05$) from zero only for ammonium (12.7 ± 3.5 [s.e.] μmol per gram per hour) while nitrate, nitrite and phosphate showed large variations in

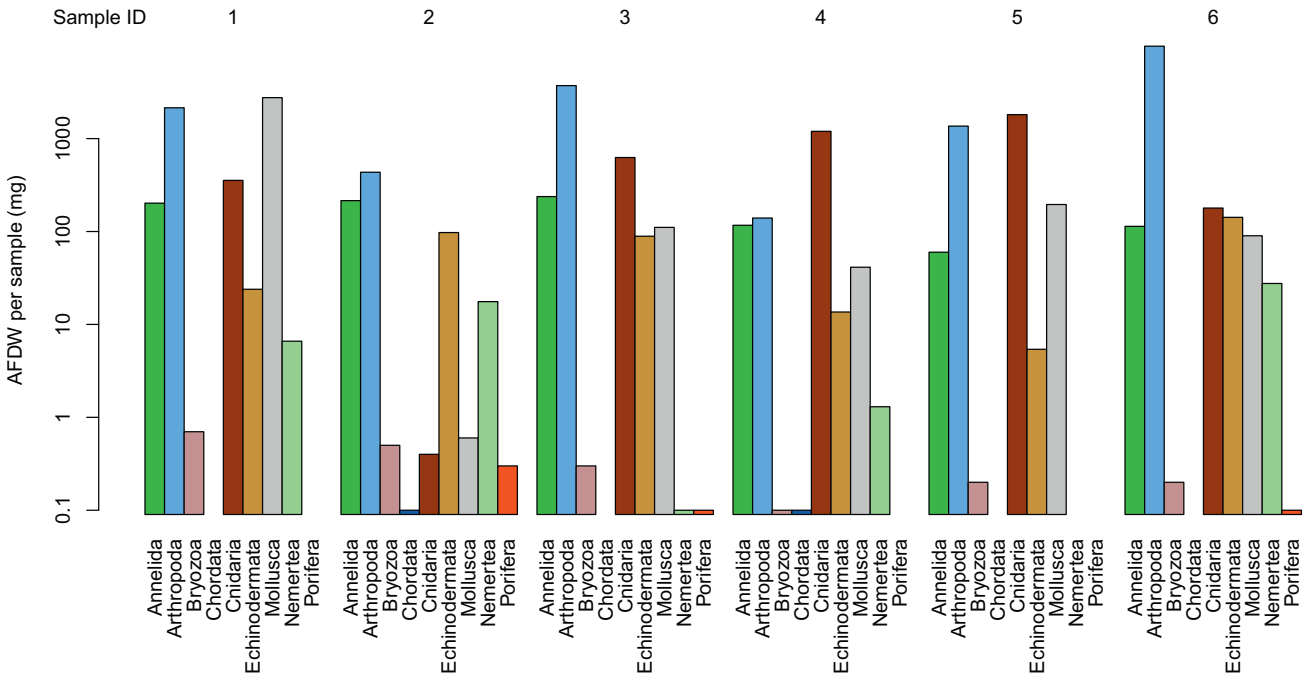

Fig. 4. Ash free dry weight (mg; in log scale) of taxonomic groups in different samples (Sample ID).

both direction and size of the fluxes, resulting in non-significant flux-weight relations .The mean flux per individual was significant for ammonium and nitrite only (Tables 3 & 4). The complete oxygen and nutrient dataset is available as online supplement S2 and all regression model results underlying Fig. 5 are available as S3.

4. Discussion

The presence of fouling fauna escalates respiration rates, regeneration rates of ammonium and phosphate and remineralisation processes (Falcão et al., 2007; Wilking et al., 2023). This was also observed in our results. In this study, we performed the first offshore in situ incubations of fouling macrofauna present on shipwrecks in the southern North Sea. The incubations showed reductions in oxygen concentration (on average $11.8*10^3$ μmol m^{-2} h^{-1}), with the highest oxygen decrease in samples having the greatest biomass. Based on four water samples per incubation, we mostly observed a clear increase in ammonium, nitrite, and phosphate. Patterns in nitrate are less unambiguous, with a small net positive flux of nitrate in two incubations and no significant flux direction for nitrate in four incubations.

The range of oxygen consumption measured in the six dome incubations was in the same order of magnitude as incubations performed on oyster reefs in Maryland and Virginia (US; Jackson et al., 2018; Volaric et al., 2018; Table 5). This indicates artificial and biogenic reefs have similarly high metabolic rates. The metabolic fluxes found in our study were higher than deep-sea coral reef fluxes in the Northeast Atlantic (de Froe et al., 2019). This could be attributed to the much lower water temperatures, lower supply of organic matter, and thus lower metabolic rates in deep waters compared to the shallow (~30 m depth) waters of the southern North Sea. On the other hand, the oxygen fluxes of our study were found to be between 4 and 124 times higher than the fluxes in sandy sediment in the North Sea, including locations in the region of our study sites (Boon et al., 1999; Braeckman et al., 2014; Conley et al., 1997; De Borger et al., 2021a; Toussaint et al., 2021).

Both biogenic and artificial shallow water reefs are clear hotspots of metabolic activity, when compared to the surrounding soft sediment habitats. This could be explained by the presence of the fouling fauna, which is linked to increased metabolic rates (Wilking et al., 2023). Furthermore, the increased metabolic activity likely contributes to nutrient cycling, e.g., increasing fluxes of ammonium and other nutrients. This is shown by the high fluxes of ammonium in our study, which overlap with the range of fluxes observed on temperate oyster reefs and mussel beds (Dame et al., 1991; Jackson et al., 2018; Kellogg et al., 2013). Finally, the ammonium fluxes observed in our study and at other shallow-water reefs are remarkably higher than those measured at cold-water coral reefs and sandy seabeds in most locations (de Froe et al., 2019) (Bratek et al., 2020; Conley et al., 1997; De Borger et al., 2021a), but overlap with the range of southern North Sea sediments from the same region as the wrecks (Braeckman et al., 2014; Toussaint et al., 2021). It should be noted that these sedimental fluxes originate from studies using various sediment types (muddy, fine sand, permeable sand) and from different times of the year, of which we only present the extremes (Table 5). Muddy and fine sediments, for example, show higher fluxes than permeable sediments, while fluxes throughout the year are often highest in summer (Braeckman et al., 2014).

Limited nitrite flux data were available in literature. Generally, the reported nitrite fluxes were highly variable. At a subtropical shallow coastal artificial reef, nitrite concentrations were too low to be detected and considered negligible (Wilking et al., 2023). Fluxes from temperate mussel beds were in the same order of magnitude as our measurements (Dame et al., 1991), while seabed fluxes were between 32 and 800 times lower than observed in our study (Conley et al., 1997).

Nitrate fluxes reported in literature varied between influx and efflux at mussel beds in the Wadden Sea, in the Eastern Scheldt estuary and for the seabeds in the central North Sea and Gulf of Finland (Conley et al., 1997; Dame et al., 1991; De Borger et al., 2021a). On the contrary, southern North Sea nitrate fluxes in sediments did not show such variability between influx and efflux (Bratek et al., 2020). De Borger et al. (2021a) linked the changing fluxes to variations in bioturbation rates and permeability of the sediment. Our nitrate flux range overlaps with the range of the mussel beds but is much wider than that of the seabed fluxes.

The Dutch estuarine mussel beds showed highly variable phosphate fluxes (Dame et al., 1991). Oyster beds flux ranges overlapped with our fluxes, but were overall much higher (Jackson et al., 2018; Kellogg et al., 2013). Both in our study and for oyster reefs, no significant relations between biomass and phosphate flux were reported (Jackson et al., 2018). Central North Sea incubations of sediments showed phosphate

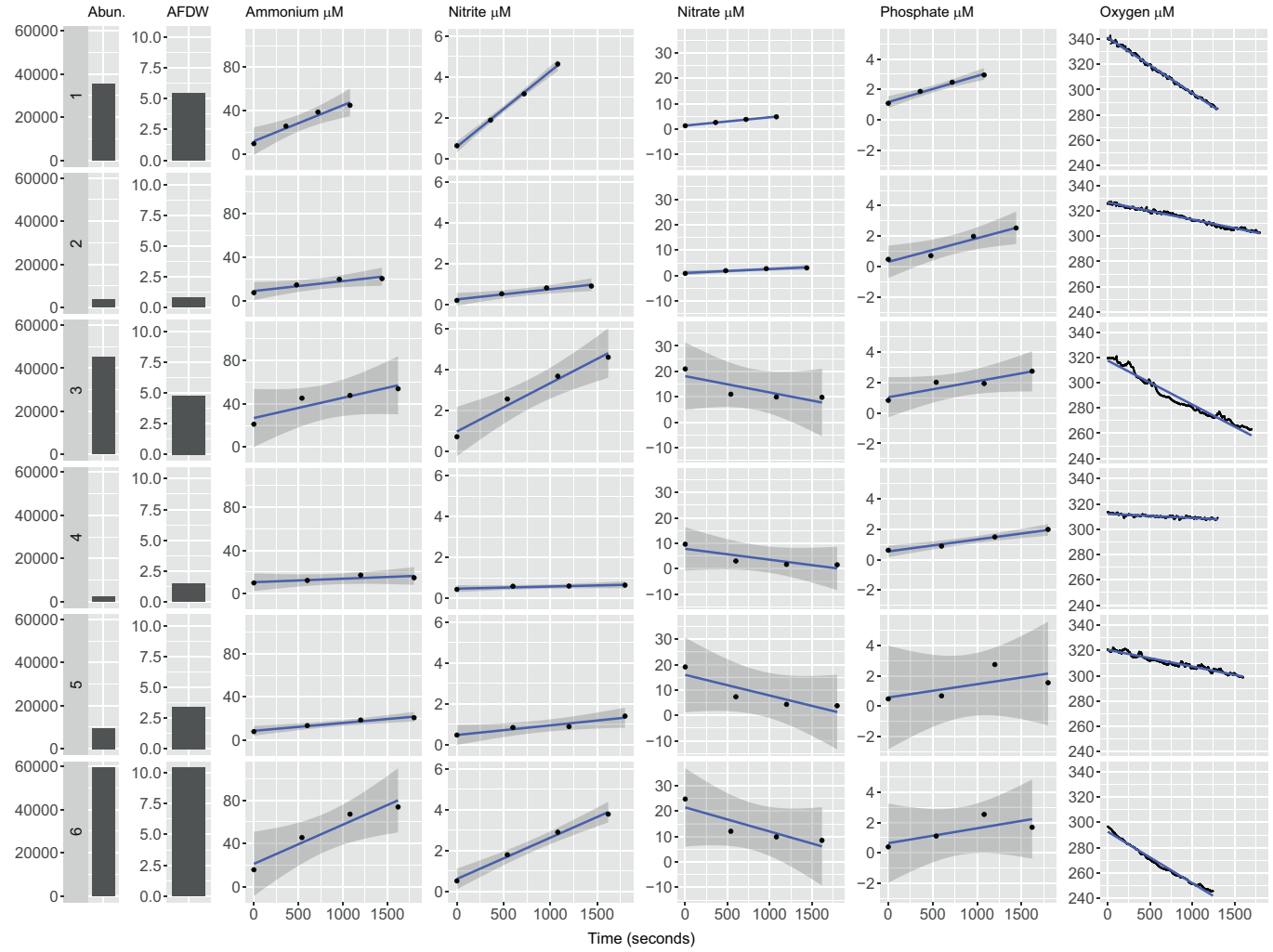

Fig. 5. Measured concentrations (µM) per sample (black dots) and modelled change during incubations (blue line) and 95% confidence intervals (grey ribbons). Rows: Sample ID, columns: 1 = abundance per sample, 2 = ash free dry weight per sample, 3 = ammonium (µM), 4 = nitrite, 5 nitrate, 6 = phosphate, 7 = oxygen. Sample ID (left grey boxes) as presented in Table 1. (For interpretation of the references to colour in this figure legend, the reader is referred to the web version of this article.)

Table 3
Summary of the mean oxygen and nutrient fluxes (Solutes) per gram of ash free dry weight, per m^2 and per individual, all in in µmol per hour and all with standard error (s.e.), *p*-value (p), adjusted-R^2 of the linear model or t-statistic (t) from the *t*-test.

Solutes	µmol per g per hr	s.e.	p	R^2	µmol per m^2 per hr	s.e.	p	t	µmol per individual per hr	s.e.	p	R^2
Δ [$NO2^-$]	0.86	0.58	0.21	0.20	80.3	30.1	0.04	2.67	$1.57*10^{-4}$	$0.69*10^{-4}$	0.08	0.46
Δ [$NO3^-$]	−2.46	2.41	0.36	0.01	−206	112	0.13	−1.84	$-2.60*10^{-4}$	$3.67*10^{-4}$	0.52	−0.11
Δ [$NH4^+$]	12.7	3.50	0.02	0.71	945	300	0.03	3.15	$1.84*10^{-3}$	$0.48*10^{-3}$	0.02	0.73
Δ [$PO4^{-3}$]	−0.035	0.20	0.87	−0.24	61.1	8.25	<0.01	7.41	$2.39*10^{-6}$	$29*10^{-6}$	0.94	−0.25
Δ [O2]	−126	47.9	0.06	0.54	$-11.8*10^3$	$3.3*10^3$	0.02	−3.59	$-2.07*10^{-2}$	$0.48*10^{-2}$	0.01	0.78

Table 4
Minimum and maximum fluxes of oxygen and nutrients in µmol per m^2 per hour.

Solute	min	max
Δ [$NO2^-$]	5.5	194
Δ [$NO3^-$]	−498	172
Δ [$NH4^+$]	169	1908
Δ [$PO4^{-3}$]	41.3	90.6
Δ [O2]	−20,809	−1530

both into and out of the sediment (De Borger et al., 2021a).

The literature-reported fluxes on temperate shallow water reefs as well as our results are consistently higher than fluxes on sandy seabeds. The higher fluxes of oxygen and nutrients on biogenic as well as artificial reefs are likely the result of much higher densities of fouling macrofauna on reef structures when compared to fauna in and on surrounding sandy sediments (Coelho et al., 2012; Coolen et al., 2020a, 2022; Lengkeek et al., 2013). Densities and weights of the fouling community show high variation on artificial structures in the North Sea, as we confirm in the present study, showing a factor 27 difference in abundance which ranged from 2187 to 59,427 between deployments. Even within the same location (Callisto wreck) the variation in abundance and AFDW

Table 5
Fluxes from literature in mmol per m^2 per hour (oxygen) and μmol per m^2 per hour (ammonium, nitrite, nitrate, phosphate).

Type	Region	Min	Max	Reference
Oxygen				
Sandy seabed	Southern North Sea	−2.9	−0.09	(Boon et al., 1999)
Sandy seabed	Central North Sea	−0.7	−0.3	(De Borger et al., 2021a)
Sandy seabed	Gulf of Finland	−0.53	−0.46	(Conley et al., 1997)
Sandy seabed	Southern North Sea	−2.3	0.0	(Braeckman et al., 2014)
Sandy seabed	Southern North Sea	−2.4	−0.57	(Toussaint et al., 2021)
Oyster reef	Maryland US	−36.9	−15.2	(Jackson et al., 2018)
Oyster reef	Virginia US	−21.3	−1.3	(Volaric et al., 2018)
Deep cold-water coral	Northeast Atlantic Ocean	−1.2	−0.2	(de Froe et al., 2019)
Shipwreck fouling	Southern North Sea	−20.8	−1.5	This study
Ammonium				
Sandy seabed	Southern North Sea	4.2	275	(Bratek et al., 2020)
Sandy seabed	Gulf of Finland	9.4	34.7	(Conley et al., 1997)
Sandy seabed	Central North Sea	−9.2	35	(De Borger et al., 2021a)
Sandy seabed	Southern North Sea	18.3	680.8	(Braeckman et al., 2014)
Sandy seabed	Southern North Sea	−79.2	1729	(Toussaint et al., 2021)
Oyster reef	Maryland US	1800	4528	(Jackson et al., 2018)
Oyster reef	Maryland US	600	3510	(Kellogg et al., 2013)
Mussel bed	Wadden Sea NL Eastern Scheldt	554	12,196	(Dame et al., 1991)
Mussel bed	NL	388	2051	(Dame et al., 1991)
Deep cold-water coral	Northeast Atlantic Ocean	0	40.8	(de Froe et al., 2019)
Shipwreck fouling	Southern North Sea	169	1908	This study
Nitrite				
Sandy seabed	Gulf of Finland	0.1	2.5	(Conley et al., 1997)
Mussel bed	Wadden Sea NL Eastern Scheldt	−195.6	282.5	(Dame et al., 1991)
Mussel bed	NL	−43.5	86.9	(Dame et al., 1991)
Shipwreck fouling	Southern North Sea	5.5	194	This study
Nitrate				
Sandy seabed	Southern North Sea	12.5	45.8	(Bratek et al., 2020)
Sandy seabed	Gulf of Finland	−6.8	12.5	(Conley et al., 1997)
Sandy seabed	Central North Sea	−8.8	23.0	(De Borger et al., 2021a)
Mussel bed	Wadden Sea NL Eastern Scheldt	−258.0	32.3	(Dame et al., 1991)
Mussel bed	NL	−80.6	354.8	(Dame et al., 1991)
Deep cold-water coral	Northeast Atlantic Ocean	15.8	85.0	(de Froe et al., 2019)
Shipwreck fouling	Southern North Sea	−498	172	This study
Phosphate				
Sandy seabed	Central North Sea	−1.7	3.8	(De Borger et al., 2021a)
Sandy seabed	Gulf of Finland	1.6	28.5	(Conley et al., 1997)
Oyster reef	Maryland US	90.0	570.0	(Kellogg et al., 2013)
Oyster reef	Maryland US	58.0	140.0	(Jackson et al., 2018)
Mussel bed	Wadden Sea NL Eastern Scheldt	−631.8	947.7	(Dame et al., 1991)
Mussel bed	NL	−84.2	2411.3	(Dame et al., 1991)
Shipwreck fouling	Southern North Sea	41	91	This study

was high. This is not uncommon on North Sea structures, where AFDW can differ by a factor of 58 between samples from the same installation (Coolen et al., 2020a).

Phosphate is mainly produced via metabolic processes of micro-organisms (Karl, 2007) while decomposing organic matter, and as such is only indirectly linked to the metabolic processes of macrofauna, during which dissolved and particulate organic phosphorus (P) would be produced. Possibly this P is not converted fast enough to show a relation with the producing macrofauna in the timeframe of our incubations. Alternatively, the variation in the conversion may be very high compared to the average change, requiring more incubations to be carried out to show a significant change. As such, the origin of the increased phosphate concentrations observed here remains unclear.

In our study, ammonium and nitrite were increasing during incubations, while nitrate was decreasing at the same time in several cases. The conversion from ammonium to nitrite and then nitrate is generally an oxic process, although anaerobic ammonium oxidation directly to N_2 as well as anoxic dissimilatory nitrate reduction to ammonium (DNRA) are also possible, while nitrate denitrification takes place under anoxic conditions, all part of the microbial nitrogen cycle (Kuypers et al., 2018). Both processes must have taken place at the same time during our incubations. Possibly anoxic conditions are present in the interstitial space between tubes built by amphipods (mainly *Jassa herdmani*). These tubes are made of "amphipod silk", consisting of mucus secretions that the amphipods are producing with their glandular pereopods (Kronenberger et al., 2012). Large numbers of these tubes together in a tight space form a thick layer of organic matter mixed with fine sediment. In some cases, these layers can have a remarkable thickness and be very compact, almost cake-like (personal observations Joop Coolen). Around burrowing polychaetes, it has been shown that fluxes of nitrate can become negative, likely as a result of anoxic conditions in the burrow wall, facilitating microbial conversion of nitrogen (Kristensen, 1985). This effect likely increases during resting periods of the polychaete, when the water in the burrow is not actively replaced. The turf layers created by amphipods observed here are likely to vary in ventilation rate and possibly an anoxic layer exists in the turf space between the Jassa tubes or in temporarily non-ventilated tubes. When actively ventilating, the amphipods would provide oxygen for the conversion of ammonium to nitrite, resulting in a nitrite increase. During non-ventilation phases inside the tubes or in the interstitial space, local anoxic conditions would allow denitrification of nitrate to N_2 or ammonium via DNRA. With thousands of amphipods present in each sample, it is likely that there is always a group of resting individuals present while others ventilate, resulting in a complex combination of oxic an anoxic turf around the amphipods, allowing both an increase of nitrite and a net decrease of nitrate in some and an increase in other incubations.

It should be noted that some initial nutrient concentrations in our incubations were rather high, in particular for the nitrate measurements with negative slopes. This may have resulted from disturbance of the fauna and Jassa turf during placement of the dome, or disturbance as a result of a change in current strength and direction inside the dome. Furthermore, the change in oxygen concentration during incubation, although only <20%, may have influenced the activity of the fauna.

Whether this behavioural change indeed takes place should be tested in future studies. In how far the variation in dome-seal compression has influenced the measurements remains unknown as this was not quantified. This may have introduced additional variation. For example: we assumed a 50% compression, but if this was 100%, the dome volume would have been approximately 800 ml lower. This would then change our results approximately 8%. Furthermore, we recommend including collection of samples from the surrounding water outside the dome at the start of future incubation and perform control incubations to estimate the magnitude of fluxes in the water column. To reduce disturbance, substrates designed to repeat dome incubations without the need to remove fauna from surrounding substrates (e.g. in the form of settlement plates) could repeatedly be measured to evaluate variation in fluxes of the same communities. Furthermore, it is recommended to investigate the small-scale oxygen climate inside the Jassa turf, e.g., using microelectrodes while incubating Jassa colonies under controlled conditions. Lastly, due to the low number of incubations we were able to perform, no attempt was made here to relate the fluxes to the faunal composition, as due to the high variation in species composition, much more data would be needed. Therefore, we recommend that future studies perform a much larger number of incubations from multiple locations, on different communities and in various seasons.

5. Conclusion

We presented the first in-situ observations of nutrient fluxes of fouling communities on artificial substrates in the North Sea. Fluxes of ammonium, nitrite, nitrate, and oxygen measured on artificial offshore structures in the southern North Sea are high compared to seabed fluxes from sandy sediments, most likely as a result of higher macrofauna densities on reefs. This is confirmed by the similarly large fluxes reported from earlier studies on shallow water temperate biogenic reefs.

The release of nitrogen and phosphate into the water column might have effects on (local) primary production. However, more datapoints should be collected with a larger temporal and spatial distribution, including repeated measurements of the same community, to be able to properly understand the effects of tens of thousands of structures in the marine environment. These combined observations would then provide vital information to improve and validate biogeochemical models that can then be used to help further improve this understanding.

CRediT authorship contribution statement

Joop W.P. Coolen: Writing – original draft, Visualization, Validation, Methodology, Investigation, Funding acquisition, Formal analysis, Conceptualization. **Babeth van der Weide:** Investigation, Data curation. **Oliver Bittner:** Investigation. **Ninon Mavraki:** Writing – review & editing, Methodology, Conceptualization. **Mandy Rus:** Writing – review & editing, Investigation, Formal analysis. **Johan van der Molen:** Writing – review & editing, Validation, Funding acquisition. **Rob Witbaard:** Writing – review & editing, Validation, Methodology, Investigation, Funding acquisition, Formal analysis, Conceptualization.

Declaration of competing interest

The authors declare the following financial interests/personal relationships which may be considered as potential competing interests:

Joop W.P. Coolen reports financial support was provided by Dutch Research Council. Johan van der Molen reports financial support was provided by Dutch Research Council. Joop W.P. Coolen reports financial support was provided by TKI Deltatechnology. If there are other authors, they declare that they have no known competing financial interests or personal relationships that could have appeared to influence the work reported in this paper.

Data availability

Data have been uploaded as supplementary material

Acknowledgements

We are grateful for the financial support provided by NWO as part of the NWA (project NWA.1236.18.001), TKI Deltatechnology and Heerema Marine Contractors by funding the ASSESS project. We thank the Dive the North Sea Clean foundation and their numerous volunteers for helping us conduct the wreck dives, Karel Bakker and Jan van Ooijen from NIOZ nutrient lab for analysing the water samples, Loran Kleine Schaars from NIOZ benthic lab for the fauna weight measurements, Edwin Keijzer and Bas Denissen from NIOZ workshop for help developing the domes, Cor Kuyvenhoven for constructing the pump housing, Joost van Uffelen for providing photos of our in-situ incubations and Jan Beermann (AWI) for advice on Jassa biology. The dome recirculation pumps were kindly provided by BLDC PUMP Technology Company Limited (China). We thank WUR colleague Enzo Kingma for providing a sketch of the dome system. We thank our anonymous reviewers for their valuable comments to the earlier version of our manuscript.

Appendix A. Supplementary data

Supplementary data to this article can be found online at https://doi.org/10.1016/j.seares.2024.102498.

References

Babcock, K.K., Cesbron, F., Patterson, W.F., Garner, S.B., Waidner, L.A., Caffrey, J.M., 2020. Changing biogeochemistry and invertebrate community composition at newly deployed aArtificial reefs in the Northeast Gulf of Mexico. Estuaries and Coasts 43 (4), 680–692. https://doi.org/10.1007/S12237-020-00713-4/FIGURES/6.

Boon, A.R., Duineveld, G.C.A., Kok, A., 1999. Benthic organic matter supply and metabolism at depositional and non-depositional areas in the North Sea. Estuar. Coast. Shelf Sci. 49, 747–761. https://doi.org/10.1006/ecss.1999.0555.

Braeckman, U., Foshtomi, M.Y., Van Gansbeke, D., Meysman, F., Soetaert, K., Vincx, M., Vanaverbeke, J., 2014. Variable importance of macrofaunal functional biodiversity for biogeochemical cycling in temperate coastal sediments. Ecosystems 17, 720–737. https://doi.org/10.1007/S10021-014-9755-7/TABLES/2.

Bratek, A., Van Beusekom, J.E.E., Neumann, A., Sanders, T., Friedrich, J., Emeis, K.-C., Dähnke, K., 2020. Spatial variations in sedimentary N-transformation rates in the North Sea (German Bight). Biogeosciences 17, 2839–2851. https://doi.org/10.5194/bg-17-2839-2020.

Burson, A., Stomp, M., Akil, L., Brussaard, C.P.D., Huisman, J., 2016. Unbalanced reduction of nutrient loads has created an offshore gradient from phosphorus to nitrogen limitation in the North Sea. Limnol. Oceanogr. 61, 869–888. https://doi.org/10.1002/LNO.10257.

Cleveland, W.S., 1985. The Elements of Graphing Data. Wadsworth Advanced Books and Software, Belmont, CA.

Coelho, R., Monteiro, P., Abecasis, D., Blot, J.Y., Gonçalves, J.M.S., 2012. Macrofauna assemblages in a XVIIth century shipwreck: comparison with those on natural reefs and sandy bottoms. Braz. J. Oceanogr. 60, 447–462.

Conley, D.J., Stockenberg, A., Carman, R., Johnstone, R.W., Rahm, L., Wulff, F., 1997. Sediment-water nutrient fluxes in the Gulf of Finland, Baltic Sea. Estuar. Coast. Shelf Sci. 45, 591–598. https://doi.org/10.1006/ECSS.1997.0246.

Coolen, J.W.P., Gittenberger, A., Schrieken, N., Lengkeek, W., 2012. Wrakken-expeditie Doggersbank 2011. Zoekbeeld 2, 22–23.

Coolen, J.W.P., Bos, O.G., Glorius, S., Lengkeek, W., Cuperus, J., van der Weide, B.E., Agüera, A., 2015. Reefs, sand and reef-like sand: a comparison of the benthic biodiversity of habitats in the Dutch Borkum Reef Grounds. J. Sea Res. 103, 84–92.

Coolen, J.W.P., Lengkeek, W., Degraer, S., Kerckhof, F., Kirkwood, R.J., Lindeboom, H.J., 2016. Distribution of the invasive Caprella mutica Schurin, 1935 and native Caprella linearis (Linnaeus, 1767) on artificial hard substrates in the North Sea: separation by habitat. Aquat. Invasions 11, 437–449.

Coolen, J.W.P., Bittner, O., Driessen, F.M.F., van Dongen, U., Siahaya, M.S., de Groot, W., Mavraki, N., Bolam, S.G., van der Weide, B., 2020a. Ecological implications of removing a concrete gas platform in the North Sea. J. Sea Res. 166, 101968 https://doi.org/10.1016/j.seares.2020.101968.

Coolen, J.W.P., Boon, A.R., Crooijmans, R.P., Van Pelt, H., Kleissen, F., Gerla, D., Beermann, J., Birchenough, S.N.R., Becking, L.E., Luttikhuizen, P.C., 2020b. Marine stepping-stones: water flow drives Mytilus edulis population connectivity between offshore energy installations. Mol. Ecol. 29, 686–703. https://doi.org/10.1111/mec.15364.

Coolen, J.W.P., van der Weide, B.E., Cuperus, J., Blomberg, M., van Moorsel, G.W.N.M., Faasse, M.A., Bos, O.G., Degraer, S., Lindeboom, H.J., 2020c. Benthic biodiversity on old platforms, young wind farms and rocky reefs. ICES J. Mar. Sci. 77, 1250–1265.

Coolen, J.W.P., Vanaverbeke, J., Dannheim, J., Garcia, C., Birchenough, S., Krone, R., Beermann, J., 2022. Generalized changes of benthic communities after construction of wind farms in the southern North Sea. J. Environ. Manag. 315, 115173.
Dame, R., Dankers, N., Prins, T., Jongsma, H., 1991. The influence of mussel beds on nutrients in the Western Wadden Sea and eastern Scheldt. Estuaries 14, 130–138.
Dannheim, J., Bergström, L., Birchenough, S.N.R., Brzana, R., Boon, A.R., Coolen, J.W.P., Dauvin, J.-C., De Mesel, I., Derweduwen, J., Gill, A.B., Hutchison, Z.L., Jackson, A. C., Janas, U., Martin, G., Raoux, A., Reubens, J., Rostin, L., Vanaverbeke, J., Wilding, T.A., Wilhelmsson, D., Degraer, S., 2020. Benthic effects of offshore renewables: identification of knowledge gaps and urgently needed research. ICES J. Mar. Sci. 77, 1092–1108. https://doi.org/10.1093/icesjms/fsz018.
Dannheim, J., Coolen, J.W.P., Vanaverbeke, J., Mavraki, N., Zupan, M., Spielmann, V., Degraer, S., Hutchison, Z., Carey, D., Rasser, M., Sheehan, E., Birchenough, S., Buyse, J., Gill, A.B., Janas, U., Teschke, K., Causon, P.L., Krone, R., van der Weide, B., Bittner, O., Faasse, M., Kloss, P., (submitted) Biodiversity Information of Benthic Species at ARtificial Structures – BISAR.
De Borger, E., Braeckman, U., Soetaert, K., 2021a. Rapid organic matter cycling in North Sea sediments. Cont. Shelf Res. 214, 104327 https://doi.org/10.1016/j.csr.2020.104327.
De Borger, E., Ivanov, E., Capet, A., Braeckman, U., Vanaverbeke, J., Grégoire, M., Soetaert, K., 2021b. Offshore windfarm footprint of sediment organic matter mineralization processes. Front. Mar. Sci. 0, 667. https://doi.org/10.3389/FMARS.2021.632243.
de Froe, E., Rovelli, L., Glud, R.N., Maier, S.R., Duineveld, G., Mienis, F., Lavaleye, M., van Oevelen, D., 2019. Benthic oxygen and nitrogen exchange on a cold-water coral reef in the north-East Atlantic Ocean. Front. Mar. Sci. 6, 482996 https://doi.org/10.3389/FMARS.2019.00665/BIBTEX.
de Vrees, L., 2019. Adaptive marine spatial planning in the Netherlands sector of the North Sea. Mar. Policy 103418. https://doi.org/10.1016/j.marpol.2019.01.007.
Degraer, S., Carey, D., Coolen, J.W.P., Hutchison, Z., Kerckhof, F., Rumes, B., Vanaverbeke, J., 2020. Offshore Wind farm artificial reefs affect ecosystem structure and functioning: a synthesis. Oceanography 33, 48–57. https://doi.org/10.5670/oceanog.2020.405.
EMODnet, 2019. European Marine Observation Data Network (EMODnet) Bathymetry portal [WWW Document]. URL. https://www.emodnet-bathymetry.eu (accessed 12.5.19).
Falcão, M., Santos, M.N., Vicente, M., Monteiro, C.C., 2007. Biogeochemical processes and nutrient cycling within an artificial reef off southern Portugal. Mar. Environ. Res. 63, 429–444. https://doi.org/10.1016/J.MARENVRES.2006.12.001.
Fowler, A.M., Jørgensen, A., Svendsen, J.C., Macreadie, P.I., Jones, D.O., Boon, A.R., Booth, D.J., Brabant, R., Callahan, E., Claisse, J.T., Dahlgren, T.G., Degraer, S., Dokken, Q.R., Gill, A.B., Johns, D.G., Leewis, R.J., Lindeboom, H.J., Linden, O., May, R., Murk, A.J., Ottersen, G., Schroeder, D.M., Shastri, S.M., Teilmann, J., Todd, V., Van Hoey, G., Vanaverbeke, J., Coolen, J.W.P., 2018. Environmental benefits of leaving offshore infrastructure in the ocean. Front. Ecol. Environ. 16, 571–578. https://doi.org/10.1002/FEE.1827.
Gmelig Meyling, A.W., Schrieken, N., Coolen, J.W.P., 2012. Drie jaar monitoring van wrakken op de Noordzee. Zoekbeeld 2, 4–18.
Grasshoff, K., Ehrhardt, M., Kremling, K., 1983. Methods of Seawater Analysis. Verlag Chemie.
Helder, W., De Vries, R.T.P., 1979. An automatic phenol-hypochlorite method for the determination of ammonia in sea- and brackish waters. Neth. J. Sea Res. 13, 154–160.
Hiscock, K., 1981. Marine life on the wreck of the MV "Robert.". In: Report of the Lundy Field Society, 32, pp. 40–44.
Holt, J.T., James, I.D., 1999. A simulation of the Southern North Sea in comparison with measurements from the North Sea project. Part 1: temperature. Cont. Shelf Res. 19, 1087–1112. https://doi.org/10.1016/S0278-4343(99)00015-1.
Hooper, T., Armstrong, A., Vlaswinkel, B., 2021. Environmental impacts and benefits of marine floating solar. Sol. Energy 219, 11–14. https://doi.org/10.1016/J.SOLENER.2020.10.010.
Hopkinson, C.S., Fallon, R.D., Jansson, B.-O., Schubauer, J.P., 1991. Community metabolism and nutrient cycling at Gray's Reef, a hard bottom habitat in the Georgia Bight*. Mar. Ecol. Prog. Ser. 73, 105–120.
Hydes, D.J., Aoyama, M., Aminot, A., Bakker, K., Becker, S., Coverly, S., Daniel, A., Dickson, A.G., Grosso, O., Kerouel, R., Van Ooijen, J., Sato, K., Tanhua, T., Woodward, E.M.S., Zhang, J.Z., 2010. Determination of dissolved nutrients (N, P, Si) in seawater with high precision and inter-comparability using gas-segmented continuous flow analysers. In: The GO-SHIP Repeat Hydrography Manual: A Collection of Expert Reports and Guidelines. IOCCP Report No 14, ICPO Publication Series No. 134, Version 1, 2010, pp. 1–87.
Jackson, M., Owens, M.S., Cornwell, J.C., Lisa Kellogg, M., 2018. Comparison of methods for determining biogeochemical fluxes from a restored oyster reef. PLoS One 13. https://doi.org/10.1371/journal.pone.0209799.
Jansen, H.M., Van Den Burg, S., Bolman, B., Jak, R.G., Kamermans, P., Poelman, M., Stuiver, M., 2016. The feasibility of offshore aquaculture and its potential for multi-use in the North Sea. Aquac. Int. 24, 735–756. https://doi.org/10.1007/S10499-016-9987-Y/TABLES/4.
Karl, D.M., 2007. The marine phosphorus cycle. In: Manual of Environmental Microbiology, pp. 523–539.
Kellogg, M.L., Cornwell, J.C., Owens, M.S., Paynter, K.T., 2013. Denitrification and nutrient assimilation on a restored oyster reef. Mar. Ecol. Prog. Ser. 480, 1–19. https://doi.org/10.3354/MEPS10331.
Kerckhof, F., Coolen, J.W.P., Rumes, B., Degraer, S., 2018. Recent findings of wild European flat oysters *Ostrea edulis* (Linnaeus, 1758) in Belgian and Dutch offshore waters: new perspectives for offshore oyster reef restoration in the southern North Sea. Belg. J. Zool. 148, 13–24.
Kristensen, E., 1985. Oxygen and inorganic nitrogen exchange in a "Nereis virens" (Polychaeta) Bioturbated sediment-water system. Source. J. Coast. Res. 1, 109–116.
Krone, R., Schröder, A., 2011. Wrecks as artificial lobster habitats in the German bight. Helgol. Mar. Res. 65, 11–16. https://doi.org/10.1007/s10152-010-0195-2.
Krone, R., Gutow, L., Joschko, T.J., Schröder, A., 2013. Epifauna dynamics at an offshore foundation-implications of future wind power farming in the North Sea. Mar. Environ. Res. 85, 1–12. https://doi.org/10.1016/j.marenvres.2012.12.004.
Kronenberger, K., Moore, P.G., Halcrow, K., Vollrath, F., 2012. Spinning a marine silk for the purpose of tube-building. J. Crustac. Biol. 32, 191–202. https://doi.org/10.1163/193724011X615532.
Kuypers, M.M.M., Marchant, H.K., Kartal, B., 2018. The microbial nitrogen-cycling network. Nat. Rev. Microbiol. 16, 263–276. https://doi.org/10.1038/nrmicro.2018.9.
Leewis, R.J., Waardenburg, H.W., 1991. Environmental impact of shipwrecks in the North Sea. I. Positive effects: Epifauna of North Sea shipwrecks. Water Sci. Technol. 24, 297–298.
Lengkeek, W., Coolen, J.W.P., Gittenberger, A., Schrieken, N., 2013. Ecological relevance of shipwrecks in the North Sea. Nederlandse Faunistische Mededelingen 40, 49–58.
Li, C., Coolen, J.W.P., Scherer, L., Mogollón, J.M., Braeckman, U., Vanaverbeke, J., Tukker, A., Steubing, B., 2023. Offshore Wind energy and marine biodiversity in the North Sea: life cycle impact assessment for benthic communities. Environ. Sci. Technol. 57, 6455–6464. https://doi.org/10.1021/acs.est.2c07797.
Luttikhuizen, P., Beermann, J., Crooijmans, R., Jak, R., Coolen, J.W.P., 2019. Low genetic connectivity in a fouling amphipod among man-made structures in the southern North Sea. Mar. Ecol. Prog. Ser. 133–142 https://doi.org/10.3354/meps12929.
Massin, C., Norro, A., Mallefet, J., 2002. Biodiversity of a wreck from the Belgian continental shelf: monitoring using scientific diving: preliminary results. Bulletin van het Koninklijk Belgisch Instituut voor Natuurwetenschappen. Biologie= Bulletin de l'Institut Royal des Sciences Naturelles de Belgique. Biologie 72.
Mavraki, N., Degraer, S., Vanaverbeke, J., Braeckman, U., 2020a. Organic matter assimilation by hard substrate fauna in an offshore wind farm area: a pulse-chase study. ICES J. Mar. Sci. 77, 2681–2693. https://doi.org/10.1093/icesjms/fsaa133.
Mavraki, N., De Mesel, I., Degraer, S., Moens, T., Vanaverbeke, J., 2020b. Resource niches of co-occurring invertebrate species at an offshore wind turbine indicate a substantial degree of trophic plasticity. Front. Mar. Sci. 7 https://doi.org/10.3389/fmars.2020.00379 Offshore.
Mavraki, N., Coolen, J.W.P., Kapasakali, D.A., Degraer, S., Vanaverbeke, J., Beermann, J., 2022. Small suspension-feeding amphipods play a pivotal role in carbon dynamics around offshore man-made structures. Mar. Environ. Res. 178 https://doi.org/10.1016/j.marenvres.2022.105664.
McLean, D.L., Ferreira, L.C., Benthuysen, J.A., Miller, K.J., Schläppy, M., Ajemian, M.J., Berry, O., Birchenough, S.N.R., Bond, T., Boschetti, F., Bull, A.S., Claisse, J.T., Condie, S.A., Consoli, P., Coolen, J.W.P., Elliott, M., Fortune, I.S., Fowler, A.M., Gillanders, B.M., Harrison, H.B., Hart, K.M., Henry, L., Hewitt, C.L., Hicks, N., Hock, K., Hyder, K., Love, M., Macreadie, P.I., Miller, R.J., Montevecchi, W.A., Nishimoto, M.M., Page, H.M., Paterson, D.M., Pattiaratchi, C.B., Pecl, G.T., Porter, J. S., Reeves, D.B., Riginos, C., Rouse, S., Russell, D.J.F., Sherman, C.D.H., Teilmann, J., Todd, V.L.G., Treml, E.A., Williamson, D.H., Thums, M., 2022. Influence of offshore oil and gas structures on seascape ecological connectivity. Glob. Chang. Biol. https://doi.org/10.1111/gcb.16134.
Motoda, S., 1959. Devices of simple plankton apparatus. In: Memoirs of the Faculty of Fisheries Hokkaido University, 7, pp. 73–94.
Murphy, J., Riley, J.P., 1962. A modified single solution method for the determination of phosphate in natural waters. Anal. Chim. Acta 27, 31–36.
Nall, C.R., Schläppy, M.L., Guerin, A.J., 2017. Characterisation of the biofouling community on a floating wave energy device. Biofouling. https://doi.org/10.1080/08927014.2017.1317755.
Peeters, J.C.H., Peperzak, L., 1990. Nutrient limitation in the North Sea: a bioassay approch. Neth. J. Sea Res. 26, 61–73. https://doi.org/10.1016/0077-7579(90)90056-M.
R Core Team, 2022. R: A language and environment for statistical computing (Version 4.2.1).
Rijkswaterstaat, 2024. Rijkswaterstaat Waterinfo Versie: 3.0.7 [WWW Document]. URL. https://waterinfo.rws.nl/ (accessed 2.29.24).
RStudio, 2022. RStudio (version 2022.07.0).
Schutter, M., Dorenbosch, M., Driessen, F.M.F., Lengkeek, W., Bos, O.G., Coolen, J.W.P., 2019. Oil and gas platforms as artificial substrates for epibenthic North Sea fauna: effects of location and depth. J. Sea Res. 101782 https://doi.org/10.1016/J.SEARES.2019.101782.
Slavik, K., Lemmen, C., Zhang, W., Kerimoglu, O., Klingbeil, K., Wirtz, K.W., 2019. The large-scale impact of offshore wind farm structures on pelagic primary productivity in the southern North Sea. Hydrobiologia 845, 35–53. https://doi.org/10.1007/s10750-018-3653-5.
Smith, J.M., Chavez, F.P., Francis, C.A., 2014. Ammonium uptake by phytoplankton regulates nitrification in the Sunlit Ocean. PLoS One 9, 108173. https://doi.org/10.1371/JOURNAL.PONE.0108173.
Toussaint, E., De Borger, E., Braeckman, U., De Backer, A., Soetaert, K., Vanaverbeke, J., 2021. Faunal and environmental drivers of carbon and nitrogen cycling along a permeability gradient in shallow North Sea sediments. Sci. Total Environ. 767, 144994 https://doi.org/10.1016/j.scitotenv.2021.144994.
van der Stap, T., Coolen, J.W.P., Lindeboom, H.J., 2016. Marine fouling assemblages on offshore gas platforms in the southern North Sea: effects of depth and distance from

shore on biodiversity. PLoS One 11, 1–16. https://doi.org/10.1371/journal.pone.0146324.
Vanaverbeke, J., Coolen, J.W.P., Harrald, M., Culloch, R., Tait, A., Rumes, B., Sparling, C., Wright, K., Murray, R.O., Evans, T., Hunt, W., Gill, A.B., Hutchison, Z., Buyse, J., Brabant, R., Bald, J., Wood, D., Warnas, M., Salvany, L., 2019. Working Group on Marine Benthal Renewable Developments (WGMBRED).
Vlaswinkel, B., Roos, P., Nelissen, M., 2023. Environmental observations at the first offshore solar farm in the North Sea. Sustainability 15, 6533. https://doi.org/10.3390/SU15086533.
Voet, Helena, Soetaert, K., Moens, T., Bodé, S., Boeckx, P., Van Colen, C., Vanaverbeke, J., 2023a. N2O production by mussels: quantifying rates and pathways in current and future climate settings. Front. Mar. Sci. 10 https://doi.org/10.3389/FMARS.2023.1101469/FULL.
Voet, H., Vlaminck, E., Van Colen, C., Bodé, S., Boeckx, P., Degraer, S., Moens, T., Vanaverbeke, J., Braeckman, U., 2023b. Organic matter processing in a [simulated] offshore wind farm ecosystem in current and future climate and aquaculture scenarios. Sci. Total Environ. 857, 159285 https://doi.org/10.1016/J.SCITOTENV.2022.159285.
Volaric, M.P., Berg, P., Reidenbach, M.A., 2018. Oxygen metabolism of intertidal oyster reefs measured by aquatic eddy covariance. Mar. Ecol. Prog. Ser. 599, 75–91. https://doi.org/10.2307/26503104.
Weiss, R.F., 1970. The solubility of nitrogen, oxygen and argon in water and seawater. Deep-Sea Res. Oceanogr. Abstr. 17, 721–735. https://doi.org/10.1016/0011-7471(70)90037-9.
Wickham, H., 2009. ggplot2: Elegant graphics for data analysis.
Wilking, L.E., Dillon, K.S., Rakocinski, C.F., 2023. Artificial reef biofouling community impacts on ecosystem metabolism and biogeochemical cycling in estuarine waters of the northern Gulf of Mexico. Estuar. Coast. Shelf Sci. 295, 108555 https://doi.org/10.1016/J.ECSS.2023.108555.
Witt, M.J., Sheehan, E.V., Bearhop, S., Broderick, A.C., Conley, D.C., Cotterell, S.P., Crow, E., Grecian, W.J., Halsband, C., Hodgson, D.J., Hosegood, P., Inger, R., Miller, P.I., Sims, D.W., Thompson, R.C., Vanstaen, K., Votier, S.C., Attrill, M.J., Godley, B.J., 2012. Assessing wave energy effects on biodiversity: the wave hub experience. Trans. R. Soc. A 370, 502–529. https://doi.org/10.1098/rsta.2011.0265.
World Forum Offshore Wind, 2023. Global Offshore Wind Report 2022.
WoRMS Editorial Board, 2022. World Register of Marine Species.
Xu, Z., Zhang, H., Wang, Y., Wang, X., Xue, S., Liu, W., 2022. Dynamic detection of offshore wind turbines by spatial machine learning from spaceborne synthetic aperture radar imagery. J. King Saud Univ. Comput. Inform. Sci. 34, 1674–1686. https://doi.org/10.1016/J.JKSUCI.2022.02.027.
Zhang, T., Tian, B., Sengupta, D., Zhang, L., Si, Y., 2021. Global offshore wind turbine dataset. Sci. Data 8, 1–12. https://doi.org/10.1038/s41597-021-00982-z.
Zintzen, V., Massin, C., Norro, A., Mallefet, J., 2006. Epifaunal inventory of two shipwrecks from the Belgian continental shelf. Hydrobiologia 555, 207–219. https://doi.org/10.1007/s10750-005-1117-1.
Zupan, M., Rumes, B., Vanaverbeke, J., Degraer, S., Kerckhof, F., 2023. Long-term succession on offshore wind farms and the role of species interactions. Diversity (Basel) 15, 288. https://doi.org/10.3390/d15020288.
Zuur, A.F., Ieno, E.N., Elphick, C.S., 2010. A protocol for data exploration to avoid common statistical problems. Methods Ecol. Evol. 1, 3–14. https://doi.org/10.1111/j.2041-210X.2009.00001.x.